American Mineralogist, Volume 61, pages 987–995, 1976

The crystal structure of hopeite

RODERICK J. HILL[1] AND J. B. JONES

Department of Geology and Mineralogy
The University of Adelaide, Adelaide, South Australia

Abstract

The crystal structure of hopeite, $Zn_3(PO_4)_2 \cdot 4H_2O$, has been solved by the Heavy Atom method from 1421 graphite-monochromatized Mo$K\alpha$ data and refined by full matrix least-squares to $R = 0.026$ ($R_w = 0.036$). The structure is orthorhombic, *Pnma*, $a = 10.597(3)$, $b = 18.318(8)$, $c = 5.031(1)$ Å, and $Z = 4$. The Zn atoms occur in two crystallographically distinct sites, one six-coordinated and deficient in Zn, the other four-coordinated. The α and β modifications of this mineral are discussed in relation to its thermal dehydration and infrared absorption properties.

Introduction

Following the discovery of abundant material on a bone breccia in a cave at the Broken Hill mine, Zambia (Spencer, 1908), the mineral hopeite, $Zn_3(PO_4)_2 \cdot 4H_2O$, has been the subject of considerable study. Much of this research has centered on the characterization of the α and β modifications first proposed by Spencer (1908) on the basis of differences in optics, density, and thermal behavior. Although most studies of the P_2O_5–ZnO–H_2O system support the existence of two varieties of hopeite displaying different optical and/or thermal properties, the characterization of these phases remains in a state of disarray: Takahashi *et al.* (1972) suggested that the α form of hopeite occurs in nature, while the β form corresponds to specimens prepared in the laboratory; Goloshchapov and Filatova (1969) seem to have been able to prepare both forms; the material synthesized by Nriagu (1973) has been identified as α-hopeite.

Two-dimensional crystal structure analyses of various natural and synthetic hopeite specimens were completed by Mamedov *et al.* (1961), Gamidov *et al.* (1963), and Liebau (1962, 1965), but the topology of the structure was not confirmed until three-dimensional studies of synthetic hopeite (Kawahara *et al.*, 1972, 1973) and of natural material (Whitaker, 1975) were published: this latter work came to our attention only after the refinement detailed in the present study was completed.

[1] Present address: Department of Geological Sciences, Virginia Polytechnic Institute and State University, Blacksburg, Virginia 24061

Experimental

Unit-cell dimensions for natural hopeite from Broken Hill, Zambia, (obtained through the courtesy of the South Australian Museum) were determined by a least-squares fitting (Appleman and Evans, 1973) of calculated to observed *d*-spacings; the data were collected at 21°C by powder diffractometry using LiF monochromatized Cu$K\alpha$ radiation ($\lambda = 1.5418$ Å), and Si powder ($a = 5.4305$ Å) as an internal standard. These and other physical constants for hopeite are: $a = 10.597(3)$[2], $b = 18.318(8)$, $c = 5.031(1)$ Å, $V = 976.60$ Å^3, formula weight = 458.1, $F(000) = 896e$, D_m (toluene immersion) = 3.065(9) g.cm^{-3}, D_x (for $Z = 4$) = 3.116 g.cm^{-3}, $\mu_{MoK\alpha} = 79.49$ cm^{-1}.

Two approximately cubic cleavage fragments, of dimensions 0.20 mm and 0.25 mm, were mounted about a^* and c^* respectively on a Stoe equi-inclination automated diffractometer. A total of 2797 reflections consistent with space group *Pn.a* (suggested from systematic absences) were measured (*a* axis, 0*kl*–12*kl*; *c* axis, *kh*0–6) of which 97 percent were within the positive octant of the reflecting sphere. The data set was collected at 21°C with graphite-monochromatized Mo$K\alpha$ radiation ($\lambda = 0.7107$ Å), utilizing the ω-scan technique: details of the procedure are described by Snow (1974).

Absorption corrections were applied to the data collected from each crystal using a local modification of the program ABSCOR (Busing and Levy, 1957). Lorentz and polarization corrections were then applied, incorporating functions appropriate for use

[2] e.s.d.'s given in parentheses, refer to the last decimal place.

with a highly mosaic monochromator (Whittaker, 1953). Statistical tests (Howells *et al.*, 1950; Ramachandran and Srinivasan, 1959) carried out on the distribution of diffracted intensities confirmed the space group as $Pnma$, rather than $Pn2_1a$, and the data were then scaled together by a non-iterative least-squares method (Rae, 1965) to yield 1421 unique reflections. Of these data, 88 had intensities less than three times the standard deviation of the counting statistics and were considered to be "unobserved"; they were assigned a theoretical value and standard deviation according to Hamilton (1955).

Structure determination and refinement

The two Zn atoms in the hopeite asymmetric unit were located from the Patterson function, and the P and O atoms from Fourier syntheses. These atoms were refined by least-squares minimization of the function $\Sigma w(|F_o| - |F_c|)^2$, where F_o and F_c are the observed and calculated structure factors, and the weights (w) are derived from counting statistics. Refinement with isotropic temperature factors converged with a conventional R index of 0.076. Refinement[3] with anisotropic temperature factors incorporating the symmetry restrictions of Levy (1956) for the three atoms in special positions, and the inclusion of a secondary extinction parameter, G, (described by Hill, 1976) further reduced R to 0.053. Transfer to a unity weighting scheme removed all traces of nonlinearity (at high intensity) in a plot of $\Sigma w(|F_o| - |F_c|)^2$ *vs.* $|F_c|$, the refinement converging to an R value of 0.0371 and R_w[4] = 0.044. The value of G was $5.9(5) \times 10^{-5} e^{-2}$.

Zn nonstoichiometry

During our unsuccessful attempts to locate feasible sites for the hydrogen atoms from the distribution of residual electron density it was found that the major peak ($-1.8e$ Å^{-3}) occurred at the Zn(1) location. This apparent excess of input scattering matter suggested that the Zn(1) atom may have been occupying more than one of the (four) face-sharing octahedra of O atoms at $y = 1/4$ in the asymmetric unit. However, the difference maps were completely featureless in the regions of the three vacant octahedron centers, and a least-squares cycle in which the site occupancy parameters (alone) of all four sites were released simultaneously yielded values insignificantly different from their input (ordered) contents. Moreover, examination of the secondary X-ray spectrum of hopeite produced by the 20 kV electron beam of an ETEC Scanning Electron Microscope failed to indicate the presence of any element (other than Zn and P) in sufficient amount to account for the observed difference between input and calculated scattering matter at the Zn(1) site. These results prompted the following experiments designed to test whether hopeite is nonstoichiometric.

(1) *Site occupancy refinement of the Zn atoms.* During one cycle of full matrix least-squares refinement the occupancy of the (octahedral) Zn(1) site dropped to 0.874(4) and that of the (tetrahedral) Zn(2) site to 0.984(3). Changes to all other parameters (except some temperature factors) were smaller than their associated errors, but the R factor had dropped from 0.0371 to 0.0264. An equivalent cycle using scattering factors appropriate to Zn^{2+} (instead of neutral atom) produced occupancies of 0.869(4) and 0.986(3) for Zn(1) and Zn(2) respectively, demonstrating that the changes in occupancy were independent of ionization effects. The marked decrease in Zn(1) site occupancy in the face of a minor change in Zn(2) occupancy, and a low (0.35) correlation coefficient between these parameters is believed to represent a real response of the Zn(1) occupancy parameter to the excess of input scattering matter at this site. Since no other atomic position in the asymmetric unit was observed with a significant level of residual electron density, no attempt was made to refine the site occupancies of any of the other atoms. In fact, the refinement was continued with the Zn(2) occupancy also fixed at 1.0. Upon convergence, the Zn(1) site occupancy had dropped to 0.868(2), the R value was 0.0263, with $R_w = 0.036$ ($R = 0.028$ and $R_w = 0.037$ with the inclusion of unobserved reflections), and there was a significant reduction in the magnitudes of the parameter standard errors and difference-map peaks.

(2) *Density measurements.* The accuracy and precision of the Berman balance used for the density measurements was tested on several euhedral quartz crystals and produced a mean value of 2.657(6) g.cm^{-3}. This value is in close agreement with the accepted (Frondel, 1962) density of colorless quartz at 25°C (2.658 g.cm^{-3}). Measurements on twelve hopeite crystals from Zambia with weights in the range 20–85 mg gave a mean value of 3.065(9) g.cm^{-3}. These results are in agreement with the values obtained by Spencer (1908) but are significantly lower than the calculated density (3.116 g.cm^{-3}) of hopeite based on

[3] The form of the anisotropic thermal ellipsoid is $\exp[-(\beta_{11}h^2 + \beta_{22}k^2 + \beta_{33}l^2 + 2\beta_{12}hk + 2\beta_{13}hl + 2\beta_{23}kl)]$.

[4] $R_w = [\Sigma w(|F_o| - |F_c|)^2/\Sigma wF_o^2]^{1/2}$

the ideal formula $Zn_3(PO_4)_2 \cdot 4H_2O$. Even the consistently larger cell dimensions quoted by Whitaker (1975) yield a value (3.096) which is significantly higher than the observed density in this study.

Using the estimate of Zn(1) site occupancy obtained during crystal structure analysis as an indication of the level of Zn deficiency, the calculated density of hopeite of composition $Zn_{2.868}(PO_4)_2 \cdot 4H_2O$ is 3.057 g.cm^{-3}, in good agreement with the observed value. Moreover, the average of Spencer's chemical analyses yield a formula $Zn_{2.89}P_{2.03}O_8 \cdot 4.07H_2O$, and he himself notes ". . . like almost all analyses of artificial hopeite they show slight variations from the theoretical values. The same differences are not shown in the analyses of parahopeite. . . ." In fact, the observed density (3.109) for synthetic hopeite (de Schulten, 1904) yields a formula $Zn_{2.91}(PO_4)_2 \cdot 4H_2O$ when the cell dimensions determined for this material (Kawahara *et al.*, 1973) are used.

(3) *Electron microprobe analysis.* Several crystals of natural hopeite from Zambia were analyzed with an ARL EMX microprobe using the EMPADR VII computer program of Rucklidge and Gasparrini (1969) for data reduction. Standards used were apatite (P) and adamite (Zn) from Durango, Mexico.

Five analyses, each representing a total counting time of 100 seconds for both Zn and P, yielded average weight percentages ZnO = 50.3, P_2O_5 = 32.3, and H_2O (by difference) = 17.4, and a formula $Zn_{2.82}P_{2.07}O_8 \cdot 4.3H_2O$. The results are in approximate agreement with the level of nonstoichiometry suggested from the X-ray refinement, and correspond to a density of 3.087 g.cm^{-3} (3.050 if the formula is assumed to contain exactly four molecules of water).

In the light of the above observations, it seems very probable that natural hopeite from Broken Hill, Zambia, (and also synthetic material) has a deficiency of Zn in the octahedral site. Therefore the refinement with the Zn(1) site occupancy factor released (R = 0.0263) is presented as the final hopeite structure. The corresponding positional and thermal parameters and their standard deviations estimated from the inverted full matrix are given in Table 1. Table 2 gives the anisotropic thermal ellipsoid data (from Table 1) transformed to the parameters of dimensions (r.m.s. vibrations in Å) and orientations of principal ellipsoid axes. The observed and calculated structure factors are listed in Table 3.[5]

Scattering factors for Zn, P, and O (neutral atoms) were obtained from Cromer and Waber (1965) and were corrected for the real part of the anomalous dispersion (Cromer, 1965). Programs used for solution, refinement, and geometry calculations were local modifications of FORDAP,[6] ORFLS (Busing *et al.*, 1962), ORFFE (Busing *et al.*, 1964) and ORTEP (Johnson, 1965).

Discussion of the structure

Hopeite crystallizes with the topology displayed in Figure 1 and the bonding dimensions summarized in Table 4. The structure is dominated by the presence of puckered sheets of corner-sharing tetrahedra of O atoms perpendicular to the *b* axis, separated by sheets of face-sharing vacant and occupied O octahedra. The Zn atoms are divided in the ratio 2:1 between one-half of the tetrahedral sites and one-quarter of

[5] To obtain a copy of Table 3, order Document AM-76-026 from the Mineralogical Society of America, Business Office, 1909 K St. N.W., Washington, D.C. 20006. Please remit in advance $1.00 for a copy of the microfiche.

[6] A program to execute Fourier summations written by A. Zalkin of the University of California, Berkeley, California.

TABLE 1. Atomic coordinates and temperature factor coefficients for hopeite*

	x	y	z	β_{11}	β_{22}	β_{33}	β_{12}	β_{13}	β_{23}
Zn(1)	26365(5)	1/4	07280(11)	261(6)	129(2)	1055(23)	0	-38(8)	0
Zn(2)	14273(3)	49915(2)	20780(6)	219(3)	98(1)	887(14)	-3(1)	1(4)	-15(3)
P	39710(7)	40580(4)	22561(16)	258(6)	72(2)	932(28)	11(2)	-20(9)	17(6)
O(1) ≡ H_2O	1065(3)	3/4	2579(7)	36(3)	18(1)	139(12)	0	-8(5)	0
O(2) ≡ H_2O	1143(3)	1/4	3480(8)	28(3)	28(1)	178(14)	0	18(5)	0
O(3) ≡ H_2O	3367(3)	6695(2)	3372(6)	45(2)	16(1)	267(12)	7(1)	15(4)	4(3)
O(4)	3599(2)	3275(1)	2838(5)	55(2)	10(1)	145(9)	-8(1)	-27(4)	6(2)
O(5)	1003(3)	5795(2)	4283(5)	94(3)	13(1)	117(9)	12(1)	-23(4)	-9(2)
O(6)	0250(2)	4217(1)	1433(6)	26(2)	11(1)	259(10)	-3(1)	10(3)	-10(2)
O(7)	3013(2)	4597(1)	3597(5)	29(2)	14(1)	120(8)	6(1)	-14(3)	-11(2)

* Positional parameters and anisotropic temperature factors × 10^5 for Zn and P; × 10^4 for O. The error in the final figure is indicated in parentheses.

TABLE 2. Magnitudes and orientation of principal axes of thermal ellipsoids in hopeite

	Axis	Rms displacement (Å)*	Angle, in degrees, to +a	+b	+c
Zn(1)	1	0.114(1)	61(5)	90	29(5)
	2	0.124(1)	151(5)	90	61(5)
	3	0.148(1)	90	0	90
Zn(2)	1	0.106(1)	89(5)	83(2)	7(2)
	2	0.111(1)	176(1)	94(1)	89(5)
	3	0.130(1)	94(1)	8(1)	97(1)
P	1	0.105(2)	107(3)	48(7)	133(7)
	2	0.113(2)	80(6)	132(7)	136(7)
	3	0.123(1)	20(4)	71(4)	94(5)
O(1)	1	0.129(6)	61(13)	90	29(13)
	2	0.147(6)	151(13)	90	61(13)
	3	0.175(5)	90	0	90
O(2)	1	0.115(8)	27(6)	90	117(6)
	2	0.159(6)	117(6)	90	153(6)
	3	0.217(6)	90	0	90
O(3)	1	0.141(5)	142(4)	53(5)	82(5)
	2	0.172(5)	113(6)	131(7)	50(7)
	3	0.195(4)	62(4)	63(6)	41(7)
O(4)	1	0.112(5)	64(5)	28(10)	82(16)
	2	0.125(5)	74(8)	106(16)	23(6)
	3	0.194(3)	32(2)	112(2)	111(2)
O(5)	1	0.114(5)	88(4)	67(9)	23(9)
	2	0.137(5)	70(2)	150(7)	69(9)
	3	0.242(4)	20(2)	72(2)	99(1)
O(6)	1	0.115(5)	27(10)	63(10)	90(4)
	2	0.133(5)	65(11)	148(9)	110(3)
	3	0.188(4)	99(2)	73(3)	160(3)
O(7)	1	0.110(5)	47(20)	91(15)	43(20)
	2	0.118(5)	55(21)	127(3)	123(21)
	3	0.174(3)	63(3)	37(3)	113(3)

* Standard errors indicated in parentheses in terms of last significant figures.

the octahedral sites respectively. The other tetrahedral positions contain P, while the remaining octahedra are vacant.

In detail, the tetrahedral sheet consists of zig-zag chains of corner sharing $Zn(2)O_4$ tetrahedra running parallel to the *c* axis connected by shared corners with PO_4 groups to produce a complex sheet of three- and four-membered rings. The four-fold rings consist of alternating Zn and P tetrahedra, while the three-fold rings contain two Zn and a P tetrahedron. Distortions from tetrahedral shape in both groups are a function of the steric constraints produced by the participation of the atoms in ring formation, the effect being most strongly felt in the bonds to the trigonally coordinated O(7) atom. The O(4) atom of the PO_4 group is not involved in the ring structure, and represents the major link between the tetrahedral and octahedral sheets. It occupies a *cis* relationship with respect to the other four atoms of the octahedra (interpreted as water molecules).

The atomic coordinates reported by Whitaker (1975) are essentially identical to those presented in Table 1 of this study. However, contrary to a statement by Whitaker (1975), neither the P nor Zn tetrahedra share edges with any polyhedron of any kind: an examination of the tetrahedral sheet in Figure 1 and of the nonbonded O–O distances around P and Zn in Table 4 soon indicates that the only connections are via shared corners. Only for the $Zn(2)O_4$ group do the rather small differences in coordinates between the two refinements accrue to produce a significant difference in bond lengths, although some of this disparity may be accounted for by the slightly higher values for thermal parameters obtained in the present study (Table 2).

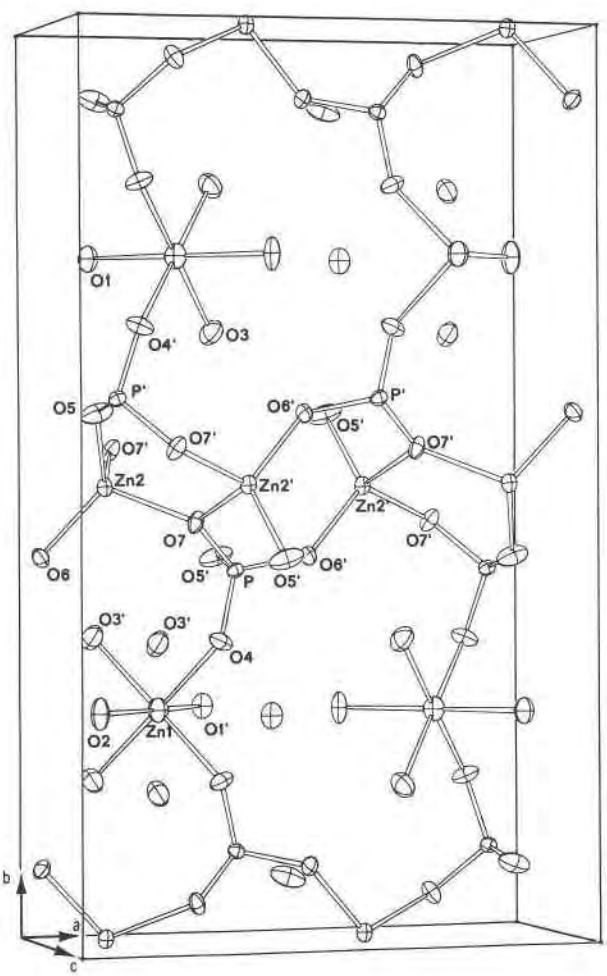

FIG. 1. Unit-cell diagram of the hopeite crystal structure (with 50% probability thermal ellipsoids). Atoms transformed outside the asymmetric unit are labelled with a superscript prime.

TABLE 4. Hopeite interatomic distances and angles*

PO_4 tetrahedron		$Zn(2)O_4$ tetrahedron		$Zn(1)O_2(H_2O)_4$ octahedron		
P–O(4)	1.516(3)	Zn(2)–O(5)	1.898(3)	Zn(1)–O(4)		2.046(3)×2
O(5)^{i}	1.520(3)	O(6)	1.918(3)	O(1)^{iii}		2.099(4)
O(6)^{ii}	1.535(3)	O(7)	1.982(2)	O(2)		2.102(4)
O(7)	1.569(3)	O(7)^{i}	1.997(2)	O(3)^{iii}		2.171(3)×2
Average =	1.535(2)	Average =	1.949(2)	Average =		2.106(2)
O(5)^{i}–O(7)	2.513(4)	O(5) –O(7)	3.078(4)	O(3)^{i} –O(3)^{iii}		2.949(6)
O(4)	2.505(4)	O(7)^{i}	3.128(4)	O(1)^{iii}		2.879(4)×2
O(6)^{ii}	2.532(4)	O(6)	3.325(4)	O(4)		3.066(4)×2
O(7) –O(4)	2.529(4)	O(7) –O(7)^{i}	3.113(3)	O(2)		3.008(5)×2
O(6)^{ii}	2.470(3)	O(6)	3.201(3)	O(1)^{iii}–O(4)		3.024(4)×2
O(4) –O(6)^{ii}	2.483(4)	O(7)^{i}–O(6)	3.185(4)	O(4) –O(4)^{iv}		2.840(5)
Average =	2.505(2)	Average =	3.172(2)	O(2)		2.982(4)×2
O(5)^{i}–P–O(7)	108.9(1)	O(5) –Zn(2)–O(7)	105.0(1)	Average =		2.976(1)
O(4)	111.2(1)	O(7)^{i}	106.9(1)	O(3)^{i} –Zn(1)–O(3)^{iii}		85.6(2)
O(6)^{ii}	111.9(2)	O(6)	121.3(1)	O(1)^{iii}		84.8(1)×2
O(7) O(4)	110.2(1)	O(7) O(7)^{i}	102.9(1)	O(4)		93.2(1)×2
O(6)^{ii}	105.5(1)	O(6)	110.3(1)	O(2)		89.5(1)×2
O(4) O(6)^{ii}	109.0(1)	O(7)^{i} O(6)	108.9(1)	O(1)^{iii} O(4)		93.7(1)×2
Average =	109.5(1)	Average =	109.2(1)	O(4) O(4)^{iv}		87.9(1)
				O(2)		91.9(1)×2
				O(1)^{iii} O(2)		172.2(1)**
				O(4) O(3)^{iii}		178.2(1)**×2
				Average =		90.0(1)

* Distances, in Å, and angles, in degrees, with e.s.d.'s given in parentheses in terms of last decimal place.

** Excluded from the average.

Symmetry transformations for atoms outside the asymmetric unit:

i. 1/2-x, 1-y, z-1/2 iii. 1/2-x, y-1/2, z-1/2

ii. 1/2+x, y, 1/2-z iv. x, 1/2-y, z

Using the data for which $\sin\theta/\lambda < 1.1$, Whitaker (1975) was able to locate three of the four hydrogen atoms in the asymmetric unit using difference syntheses, but the fourth proton position remained uncertain. In an attempt to resolve this problem the empirical bond-strength–bond-length curves of Brown and Shannon (1973) have been used to compute the balance of electrostatic charges for the (more precise) refinement reported in the present study. The results are summarized in Table 5. The extreme underbonding for O(1), O(2), and O(3) confirms that they are the oxygens of water molecules, while the moderate bond strength deficiency for O(4), O(5), and O(6) indicates that these atoms are the acceptors of hydrogen bonds from the H_2O groups.

Assuming that the hydrogen bonds are arranged within the framework so as to maintain the closest balance between valence and the sum of bond strengths received by each atom, and allocating (after Baur, 1970) 0.83 v.u. to the donor O atom and 0.17 v.u. to the acceptor atom of the hydrogen bonded group (with the four protons labelled accordingly), the scheme of bonds displayed in Table 5 may be predicted for the hopeite structure. The results corroborate the assignments made by Whitaker for H(14), H(35), and H(36), and furthermore, suggest that of his proposed positions for the fourth proton, H(24) is more likely: the alternative position, H(23), leaves O(3) overbonded, and O(4) significantly underbonded.

α and β modifications of hopeite

No X-ray evidence could be found during preliminary examinations of hopeite from Zambia for the existence of an intergrowth of two modifications, α and β, as described by Spencer (1908). However,

TABLE 5. Brown and Shannon (1973) bond-strength sums (p) for hopeite

Atom	Valence	p (without H)	Estimated bond strengths for H(14)	H(24)	H(35)	H(36)	p (with H)
Zn(1)	2	2.05					2.05
Zn(2)	2	2.01					2.01
P	5	5.00					5.00
O(1) ≡ H_2O	2	0.34	0.83(×2)				2.00
O(2) ≡ H_2O	2	0.34		0.83(×2)			2.00
O(3) ≡ H_2O	2	0.29			0.83	0.83	1.95
O(4)	2	1.69	0.17	0.17			2.03
O(5)	2	1.86			0.17		2.03
O(6)	2	1.79				0.17	1.96
O(7)	2	2.06					2.06
p for H			1.00	1.00	1.00	1.00	

polished crystal sections etched with dilute HCl displayed a "herringbone" texture (Fig. 2) similar in orientation and appearance to the growth zones documented in Spencer's work. Several workers (Goloshchapov and Filatova, 1969; Takahashi *et al.*, 1972; Kawahara *et al.*, 1972; Nriagu, 1973) have reported the presence of one or other or both of the modifications in synthetic hopeite, but as far as we are aware the present study is the first optical confirmation of their presence in natural material.

In an attempt to redefine the properties of these modifications and perhaps to explain their existence in relation to the crystal structure of the mineral, thermal dehydration and infrared absorption experiments were undertaken, as reported below.

Thermal analysis

Thermal dehydration properties were measured on a Rigaku simultaneous DTA/TGA thermo-analyzer, using AR grade α-Al_2O_3 as a standard and sample weights in the range 20–30 mg. The behavior of each sample was measured from room temperature to about 1000°C using a heating rate of 10°C/minute. Temperatures quoted were determined at maximum DTA peak height (representing deflections in the range 15–40 μV) after initial checks on various standards had confirmed the reliability of the response.

(1) *Natural hopeite.* Dehydration of a 25 mg sample of natural hopeite from Zambia, displayed in Figure 3(a),[7] proceeds in three steps, each one corresponding to the release of a nonintegral number of water molecules (Table 6). The sharp profiles of the DTA peaks (and X-ray diffraction data) are not consistent with structural disorder, but rather with the presence of a small number of quite distinct phases, each of which displays a different set of dehydration energies. Repeat analyses were very similar to Figure 3(a) but showed slight changes in both the position and magnitude of the DTA/TGA peaks.

(2) *Synthetic hopeite.* The thermal analyses presented in Figures 3(b)–(d) were carried out on samples of synthetic hopeite prepared as described by Hill (1975). In the order presented, these figures show a systematic decrease in the water lost at the low (≃128°C) and high (≃297°C) temperature steps, while the weight lost at ≃177°C increases markedly (Table 6). This sequence may be correlated with a parallel decrease in the pH of the precipitating solutions (Hill, 1975) from about 4.0 to below 2.0. On the other hand, in some samples the low-temperature peak, in turn, was completely absent from the trace. Furthermore, Goloshchapov and Filatova (1969), Kawahara *et al.* (1972) and Nriagu (1973) have obtained DTA curves which display little or no resemblance to those of Figure 3, or to each other.

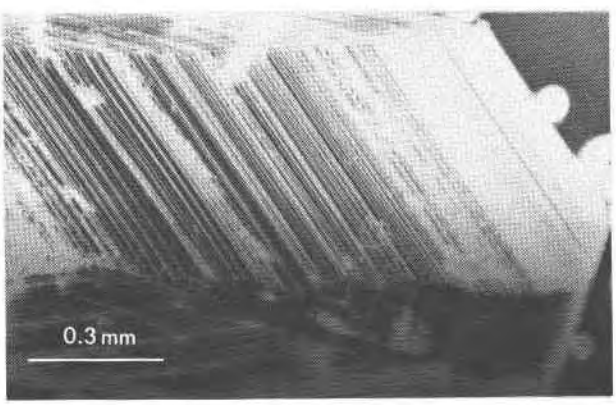

FIG. 2. Zonal growth structure in hopeite crystals etched with dilute HCl.

[7] For all analyses in Figure 3 weight loss and negative temperature differential (endothermic reaction) are plotted as downward trends, while temperature (in °C) increases from left to right.

Since the X-ray powder diffraction spectra of all samples used in this study (and presumably of samples in previous studies) are indistinguishable, it may be concluded that the nonhydrogen atom positions within the crystal structures are essentially identical and therefore that the marked differences in thermal response primarily involve changes in hydrogen atom bonding alone.

Infrared absorption spectrum

The spectrum displayed in Figure 4 was obtained on a Perkin-Elmer model 521 Grating Infrared Spectrophotometer, using a sample prepared in the manner described by Hill (1976). It was recorded in double beam mode for the region 200–4000 cm^{-1}.

The free phosphate ion belongs to point group $\bar{4}3m$, but in hopeite its site symmetry has been lowered to 1. All degeneracy of the vibrational modes is thereby lost, and the absorption spectrum is expected to display the full set of nine modes (Hertzberg, 1945; Nakamoto, 1970). In fact, only eight of these bands are visible in the spectrum of natural hopeite: 1100, 1070, 1005 cm^{-1} (all V_3), 945 cm^{-1} (V_1), 635, 585 cm^{-1} (V_4 with one peak not resolved), 350, 315 cm^{-1} (V_2). The results compare well with equivalent assignments in other phosphate minerals (Adler, 1968).

The free H_2O group has three modes of internal vibration occurring at frequencies 3652, 1640, and 3765 cm^{-1} (Hertzberg, 1945). The large peak around 1640 cm^{-1} in the hopeite spectrum corresponds to the internal bending (V_2) vibration of water molecules, while the broad, very strong band centered around 3300 cm^{-1} represents stretching (V_1 and V_3) modes, shifted to lower frequencies from their ideal values by the effects of hydrogen bonding (Farmer, 1964). In the light of the results of the thermal dehydration experiments this broad band at 3300 cm^{-1} is not surprising: it is consistent with the presence of a large variety of structurally unique H_2O groups, each with different stretching frequencies and different hydrogen bond properties. In this regard it is interesting to compare the natural hopeite spectrum in Figure 4 with that of a specimen of synthetic hopeite obtained by the Sadtler Research Laboratories using an identical spectrometer and preparation technique and included in the same figure as an insert. The absorption bands in the region of PO_4 vibrations are essentially identical, confirming the uniformity of the nonhydrogen atom framework, but the shape of the H_2O stretching region is significantly different in the two analyses, and constitutes additional evidence for the variability of hydrogen bonding schemes within the framework.

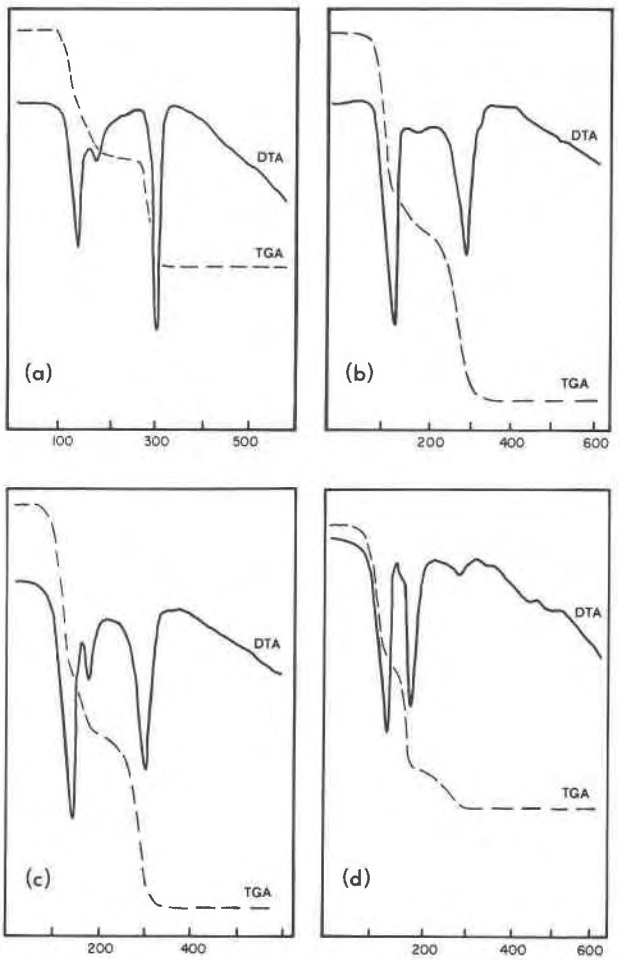

FIG. 3. Thermal dehydration characteristics of hopeite: (a) natural specimen from Zambia, (b)–(d) synthetic specimens.

Conclusions

The present work implies that both natural and synthetic material can exist in at least two, and possi-

TABLE 6. Summary of thermal dehydration characteristics of natural (N) and synthetic (S) hopeite

Sample	Figure 3	Dehydration temperatures (°C)*			Σw
N	(a)	116(1.4)	158(0.7)	296(1.8)	3.9
S	(b)	126(1.8)	184(0.4)	296(1.9)	4.1
S	(c)	134(1.7)	172(0.6)	300(1.7)	4.0
S	(d)	124(1.6)	176(1.4)	294(0.6)	3.6

* The number of water molecules (w) lost at each step from a formula unit is indicated in parentheses.

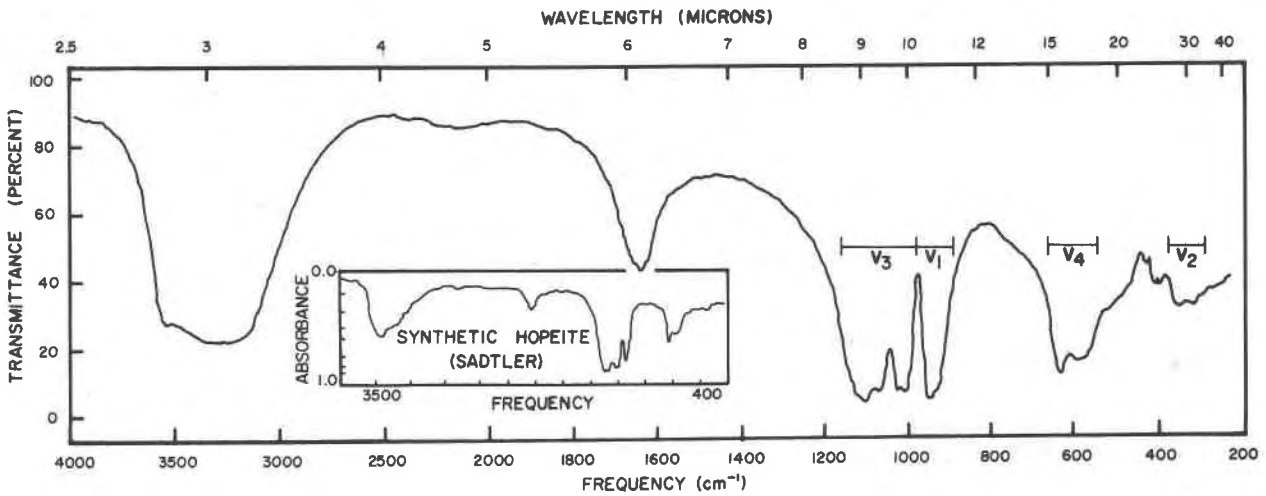

FIG. 4. Infrared absorption spectra of hopeite.

bly many more, configurations involving identical nonhydrogen atom frameworks. Spencer's α and β forms are therefore interpreted as representing the coarse intergrowth of two of these phases, the domains of which attained sufficient dimensions to allow separation by physical means. The particular form produced in nature, or in the laboratory, may depend on the specific conditions of pH and/or temperature at the time of precipitation. It is possible that these variations produce nonuniformity in optical properties as a result of changes in the polarizability of planes within the structure, thereby correlating with differences in birefringence, $2V$, and indicatrix orientation observed by Spencer, and with the "herringbone" texture reported in this study. Variations in the level of nonstoichiometry (represented by a deficiency of Zn in the octahedral site) may also play a role, perhaps in compensating for an excess of protons. Actually, the ability of the structure to incorporate a number of different hydrogen bonding schemes is not surprising when consideration is given to the sheets of vacant and occupied octahedra of O atoms and H_2O groups parallel to (010) within the hopeite framework. In fact, although synthetic hopeite possesses a topology (Kawahara *et al.*, 1973) identical to that of natural material, there are minor but significant differences between several positional parameters. These differences result in dissimilar O–H···O distances, which in turn might be expected to alter certain of the hydration energies within the structure. The small sample sizes necessary for crystal structure analysis may allow one particular phase to be isolated, but in the larger samples used for thermal dehydration experiments one would expect them to remain mixed. Whitaker (1975) suggests that the difficulty in refining the positions of atoms H(23) and H(24) in his study is a function of disorder between the two sites, but we propose the presence of at least two distinct phases (with different hydrogen bonding schemes) in the crystal he used for data collection. The inability to locate the protons in our study may be a function of the fact that the *two* crystals used to collect data each represent a different phase of natural hopeite.

Acknowledgments

The authors are especially grateful to Dr. A. R. Milnes of the Department of Earth Sciences, Monash University, Victoria, for his collaboration during the collection of the thermal analysis data, and to Mr. M. Raupach, Division of Soils, C.S.I.R.O., Adelaide, for permitting use of the IR spectrophotometer. The research was supported in part by a C.S.I.R.O. Postgraduate Studentship awarded to R.J.H.

References

ADLER, H. H. (1968) Infrared spectra of phosphate minerals: splitting and frequency shifts associated with substitution of PO_4^{3-} for AsO_4^{3-} in mimetite ($Pb_5(AsO_4)_3Cl$). *Am. Mineral.* **53,** 1740–1744.

APPLEMAN, D. E. AND H. T. EVANS, JR. (1973) Job 9214: Indexing and least-squares refinement of powder diffraction data. *Natl. Tech. Inf. Serv., U.S. Dept. Commer.*, Springfield, Virginia, Document **PB 216 188.**

BAUR, W. H. (1970) Bond length variation and distorted coordination polyhedra in inorganic crystals. *Trans. Am. Crystallogr. Assoc.* **6,** 129–155.

BROWN, I. D. AND R. D. SHANNON (1973) Empirical bond-strength–bond-length curves for oxides. *Acta Crystallogr.* **A29,** 266–282.

BUSING, W. R. AND H. A. LEVY (1957) High-speed computation of the absorption correction for single crystal diffraction measurements. *Acta Crystallogr.* **10,** 180–182.

———, K. O. MARTIN AND H. A. LEVY (1962) ORFLS, a Fortran crystallographic least-squares program. *U.S. Natl. Tech. Inform. Serv.* ORNL-TM-**305,** Oak Ridge, Tennessee.

———, ——— AND ——— (1964) ORFFE, a Fortran crystallographic function and error program. *U.S. Natl. Tech. Inform. Serv.* ORNL-TM-**306,** Oak Ridge, Tennessee.

CROMER, D. T. (1965) Anomalous dispersion corrections computed from self consistent field relativistic Dirac-Slater wave functions. *Acta Crystallogr.* **18,** 17–23.

——— AND J. T. WABER (1965) Scattering factors computed from relativistic Dirac-Slater wave functions. *Acta Crystallogr.* **18,** 104–109.

DE SCHULTEN, M. A. (1904) Production artificielle de la hopeite. *Bull. Soc. Fr. Mineral.* **27,** 100–103.

FARMER, V. C. (1964) Infra-red spectroscopy of silicates and related compounds. In, H. F. W. Taylor, Ed., *The Chemistry of Cements.* Academic Press, London.

FRONDEL, C. (1962) *The System of Mineralogy···of Dana,* Vol. III, 7th ed. John Wiley and Sons, New York, p. 115.

GAMIDOV, R. S., V. P. GOLOVACHEV, KH. S. MAMEDOV AND N. V. BELOV (1963) Crystal structure of hopeite $Zn_3[PO_4]_2 \cdot 4H_2O$. *Dokl. Akad. Nauk SSSR,* **150,** 381–384. [transl. *Dokl. Akad. Sci. USSR,* **150,** 106–109 (1965)].

GOLOSHCHAPOV, M. V. AND T. N. FILATOVA (1969) The P_2O_5–ZnO–H_2O system. *Zh. Neorg. Khim.* **14,** 814–819. [transl. *Russian J. Inorg. Chem.* **14,** 424–426 (1969)].

HAMILTON, W. C. (1955) On the treatment of unobserved reflexions in the least-squares adjustment of crystal structures. *Acta Crystallogr.* **8,** 185–186.

HERTZBERG, G. (1945) *Molecular Spectra and Molecular Structure.* Vol. 2, *Infrared and Raman Spectra of Polyatomic Molecules.* Van Nostrand, New York.

HILL, R. J. (1975) *The crystal structure of the mineral scholzite and a study of the crystal chemistry of zinc in some related phosphate and arsenate minerals.* Ph.D. Thesis, The University of Adelaide, South Australia.

——— (1976) The crystal structure and infrared properties of adamite. *Am. Mineral.* **61,** 979–986.

HOWELLS, E. R., D. C. PHILLIPS AND D. ROGERS (1950) The probability distribution of X-ray intensities. II. Experimental investigation and the X-ray detection of centres of symmetry. *Acta Crystallogr.* **3,** 210–217.

JOHNSON, C. K. (1965) ORTEP, a thermal ellipsoid plot program for crystal structure illustrations. *U.S. Natl. Tech. Inform. Serv.* ORNL-**3794,** Oak Ridge, Tennessee.

KAWAHARA, A., K. GAN, M. TAKAHASHI AND Y. TAKANO (1972) The synthesis, thermal and structural studies of hopeite. *Sci. Pap. College Gen. Ed. Univ. Tokyo,* **22,** 137–143.

——— Y. TAKANO AND M. TAKAHASHI (1973) The structure of hopeite. *Mineral. J. (Japan)* **7,** 289–297.

LEVY, H. A. (1956) Symmetry relations among coefficients of the anisotropic temperature factor. *Acta Crystallogr.* **9,** 679.

LIEBAU, F. (1962) Uber die Struktur des Hopeits, $Zn_3(PO_4)_2 \cdot 4H_2O$. *Chem. Erde,* **22,** 430–432.

——— (1965) Zur Kristallstruktur des Hopeits, $Zn_3[PO_4]_2 \cdot 4H_2O$. *Acta Crystallogr.* **18,** 352–354.

MAMEDOV, KH. S., R. GAMIDOV AND N. V. BELOV (1961) Crystal structure of hopeite, $Zn_3(PO_4)_2 \cdot 4H_2O$. *Kristallografiya,* **6,** 114–117. [transl. *Sov. Phys. Crystallogr.* **6,** 91–94 (1961)].

NAKAMOTO, K. (1970) *Infrared Spectra of Inorganic Coordination Compounds,* 2nd Ed. Wiley, New York.

NRIAGU, J. O. (1973) Solubility equilibrium constant of α-hopeite. *Geochim. Cosmochim. Acta,* **37,** 2357–2361.

RAE, A. D. (1965) The correlation of zones of X-ray intensity data from common reflections. *Acta Crystallogr.* **19,** 683–684.

RAMACHANDRAN, G. N. AND R. SRINIVASAN (1959) A new statistical test for distinguishing between centrosymmetric and noncentrosymmetric structures. *Acta Crystallogr.* **12,** 410–411.

RUCKLIDGE, J. AND E. L. GASPARRINI (1969) Specifications of a computer program for processing electron micro-probe analytical data. EMPADR VII. Toronto: Univ. Toronto, Dept. Geology, 37 p.

SNOW, M. R. (1974) The structure and absolute configuration of $(+)_{589}$-tris(biguanide)cobalt(III)trichloride monohydrate, $Co(C_2H_7N_5)_3Cl_3 \cdot H_2O$. *Acta Crystallogr.* **B30,** 1850–1856.

SPENCER, L. J. (1908) On hopeite and other zinc phosphates and associated minerals from the Broken Hill mines, North-Western Rhodesia. *Mineral. Mag.* **15,** 1–38.

TAKAHASHI, M., A. KAWAHARA AND Y. TAKANO (1972) The crystal structure of β-hopeite (abstr.). *Acta Crystallogr.* **A28,** S68.

WHITAKER, A. (1975) The crystal structure of hopeite, $Zn_3(PO_4)_2 \cdot 4H_2O$. *Acta Crystallogr.* **B31,** 2026–2035.

WHITTAKER, E. J. W. (1953) The polarisation factor for inclined-beam photographs using crystal-reflected radiation. *Acta Crystallogr.* **6,** 222–223.

Manuscript received, November 10, 1975; accepted for publication, May 12, 1976.